Integral relation in zero-pressure-gradient boundary layer flows

Tie Wei[1,*] and Joseph Klewicki[2,†]
[1]*Department of Mechanical Engineering, New Mexico Institute of Mining and Technology, Socorro, New Mexico, USA*
[2]*School of Electrical, Mechanical and Infrastructure Engineering, University of Melbourne, Parkville, Victoria, Australia*

(Received 12 July 2023; accepted 18 October 2023; published 5 December 2023)

In their 2016 paper, Wei and Klewicki [Phys. Rev. Fluids **1**, 082401 (2016)] developed an integral relation, $U_eV_e/u_\tau^2 = H_{12}$, which connects key parameters in zero-pressure-gradient (ZPG) boundary layer flows: mean velocity components U_e and V_e at the boundary layer edge, and friction velocity u_τ to shape factor H_{12}. While this relation holds exactly for ZPG laminar boundary layers featuring self-similar streamwise velocity profiles, it is an approximation for ZPG turbulent boundary layers (TBLs), with its accuracy improving as the Reynolds number increases. In this paper, we present a correction to the original integral relation, providing an exact integral relation that is applicable to ZPG boundary layer flows at arbitrary Reynolds numbers. The correction comprises two terms: one addressing deviations from self-similarity in mean streamwise velocity, and the other considering the impact of Reynolds normal stresses. Experimental and numerical data are shown to support the relative insignificance of the newly identified correction terms, except for Reynolds numbers in the transitional regime.

DOI: 10.1103/PhysRevFluids.8.124601

I. INTRODUCTION

Through an integral analysis of the mean continuity and momentum equations in the zero-pressure-gradient (ZPG) turbulent boundary layer (TBL), Wei and Klewicki [1] developed an integral equation that relates the mean velocity components at the boundary layer edge, the friction velocity, and the shape factor as follows:

$$\frac{U_eV_e}{u_\tau^2} = H_{12}. \tag{1}$$

The shape factor $H_{12} = \delta_1/\delta_2$ is significant in boundary layer flow analysis [2], as it quantifies the ratio of the mass displacement thickness δ_1 to the momentum thickness δ_2. In particular, H_{12} plays a pivotal role in characterizing mean streamwise velocity profiles and overall flow behavior [2].

It can be demonstrated that Eq. (1) holds exactly for the ZPG laminar boundary layer equations. To evaluate this integral relation within ZPG TBLs, Fig. 1 presents the direct numerical simulation (DNS) data of U_eV_e/u_τ^2 and H_{12}. In general, the behavior of U_eV_e/u_τ^2 closely mirrors that of H_{12}, demonstrating a consistent trend. Nevertheless, some noticeable differences emerge, particularly for TBLs at lower Reynolds numbers.

*tie.wei@nmt.edu
†klewicki@unimelb.edu.au

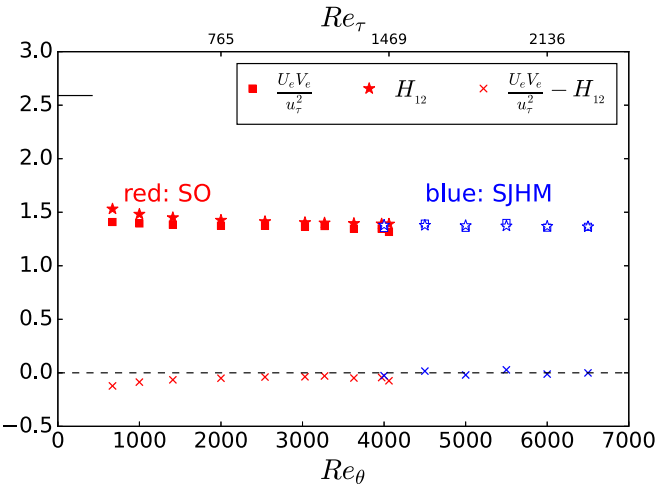

FIG. 1. Evaluating Eq. (1) with DNS data: U_eV_e/u_τ^2 and H_{12}. Re_θ and Re_τ are defined using free-stream velocity and momentum thickness, and friction velocity and boundary layer thickness, respectively. DNS data are sourced from Schlatter and Örlü [3] (SO) and Simens *et al.* [4] (SJHM).

In this paper, we present a correction to the integral relation equation (1). The analysis reveals that the correction's magnitude diminishes with increasing Reynolds numbers. As the Reynolds number tends towards infinity, Eq. (1) progressively converges to an exact relationship for ZPG TBLs.

II. INTEGRAL ANALYSIS OF ZERO-PRESSURE-GRADIENT BOUNDARY LAYER FLOWS

For statistically steady two-dimensional turbulent boundary layer flows, the governing equations of mean continuity and streamwise mean momentum can be expressed as (see, e.g., Refs. [2,5])

$$\frac{\partial U}{\partial x} + \frac{\partial V}{\partial y} = 0; \tag{2}$$

$$U\frac{\partial U}{\partial x} + V\frac{\partial U}{\partial y} = \nu\frac{\partial^2 U}{\partial y^2} + \frac{\partial R_{uv}}{\partial y} + \frac{\partial (R_{uu} - R_{vv})}{\partial x}, \tag{3}$$

where uppercase U and V denote the mean velocity components in the streamwise x and wall-normal y directions, respectively, while lowercase u and v denote the corresponding velocity fluctuations. The fluid's kinematic viscosity is denoted by ν. The kinematic Reynolds shear stress is denoted as $R_{uv} = -\langle uv \rangle$, and the kinematic Reynolds normal stresses in the streamwise and wall-normal directions are denoted as $R_{uu} = -\langle uu \rangle$ and $R_{vv} = -\langle vv \rangle$, respectively, with the angle brackets denoting the Reynolds averaging operator. The boundary layer equation for ZPG laminar flow can be obtained by setting $R_{uv} = R_{uu} = R_{vv} = 0$ in Eq. (3).

In the study of ZPG TBLs, the term $\partial(R_{uu} - R_{vv})/\partial x$ is often considered to have a negligible impact on the mean momentum equation balance, as discussed by Townsend [5]. For the sake of completeness, however, we include this term in our analysis. The corresponding boundary conditions at the wall and the boundary layer edge are summarized in Table I.

In a recent study, Wei *et al.* [6] conducted an integral analysis of the mean continuity equation (2) for ZPG boundary layers, deriving an analytical equation for the mean wall-normal velocity. The derivation employed the following normalized variables:

$$x^* \equiv \frac{x}{L}, \quad y^- \equiv \frac{y}{\delta_e}, \quad U^- \equiv \frac{U_e - U}{U_e}; \quad V^- \equiv \frac{V}{V_e}, \tag{4}$$

TABLE I. Boundary conditions for zero-pressure-gradient turbulent boundary layers at the wall and boundary layer edge.

	Boundary conditions
$y = 0$	$U = 0,\ V = 0,\ R_{uv} = 0$
$y = \delta_e$	$U = U_e,\ V = V_e,\ R_{uv} = 0$

where L represents a length scale in the streamwise direction and δ_e is the boundary layer thickness. Using the normalized variables, the $\partial U/\partial x$ term in the mean continuity equation (2) can be expressed as

$$\frac{\partial U}{\partial x} = \frac{U_e}{\delta_e}\frac{\mathrm{d}\delta_e}{\mathrm{d}x}y^- \frac{\partial U^-}{\partial y^-} - \frac{U_e}{L}\frac{\partial U^-}{\partial x^*}. \tag{5}$$

In Ref. [1], the x-derivative term $-(U_e/L)\partial U^-/\partial x^*$ in Eq. (5) was omitted. Wei *et al.* [6] included this term to obtain an analytical equation for the mean wall-normal velocity at the boundary layer edge:

$$V_e = U_e\frac{\mathrm{d}\delta_1}{\mathrm{d}x}. \tag{6}$$

Note that Eq. (6) is identical to Eq. (5.5.62) in Tennekes and Lumley's book [7], but the derivation in Ref. [7] includes unnecessary assumptions.

Applying the result for V_e, the integral analysis of the mean momentum equation introduces a correction term to the relation $U_eV_e/u_\tau^2 = H_{12}$ developed by Wei and Klewicki [1]. To simplify the integral analysis of the mean momentum equation, Eq. (3) is rewritten as

$$\frac{\partial U^2}{\partial x} + \frac{\partial (UV)}{\partial y} = \nu\frac{\partial^2 U}{\partial y^2} + \frac{\partial R_{uv}}{\partial y} + \frac{\partial (R_{uu} - R_{vv})}{\partial x}. \tag{7}$$

Upon integrating the mean momentum equation (7) in the wall-normal direction from $y = 0$ to $y = \delta_e$ and applying the appropriate boundary conditions, we arrive at

$$u_\tau^2 = -\int_0^{\delta_e}\frac{\partial U^2}{\partial x}\mathrm{d}y - U_eV_e + \int_0^{\delta_e}\frac{\partial (R_{uu} - R_{vv})}{\partial x}\mathrm{d}y. \tag{8}$$

After mathematical manipulation (see Appendixes A and B for details), the global integral of the mean momentum equation (8) can be expressed as follows:

$$\frac{U_eV_e}{u_\tau^2} = H_{12} + \frac{2\delta_1}{C_f}\frac{\mathrm{d}\ln(H_{12})}{\mathrm{d}x} - \frac{H_{12}}{u_\tau^2}\frac{\mathrm{d}}{\mathrm{d}x}\left(\delta_e u_\tau^2\int_0^1 (R_{uu}^+ - R_{vv}^+)\mathrm{d}y^-\right). \tag{9}$$

In a ZPG laminar boundary layer flow, there are no Reynolds stresses, and H_{12} is a constant due to self-similarity of the streamwise velocity profiles. Therefore Eq. (9) indicates that $U_eV_e/u_\tau^2 = H_{12}$ holds exactly for the ZPG laminar boundary layer flows.

The second and third terms on the right-hand side (RHS) of Eq. (9) serve as corrections to the integral relation developed by Wei and Klewicki in 2016 [1]. The second term emerges from the inclusion of the x-derivative term $-(U_e/L)\partial U^-/\partial x^*$ in the analysis (see Appendix A). The final term addresses the impact of Reynolds normal stresses on the mean momentum balance.

III. EVALUATION OF THE INTEGRAL EQUATION (9)

In this section, both experimental and numerical data are employed to assess the validity of the integral equation (9) and to quantify the magnitudes of the corrective terms.

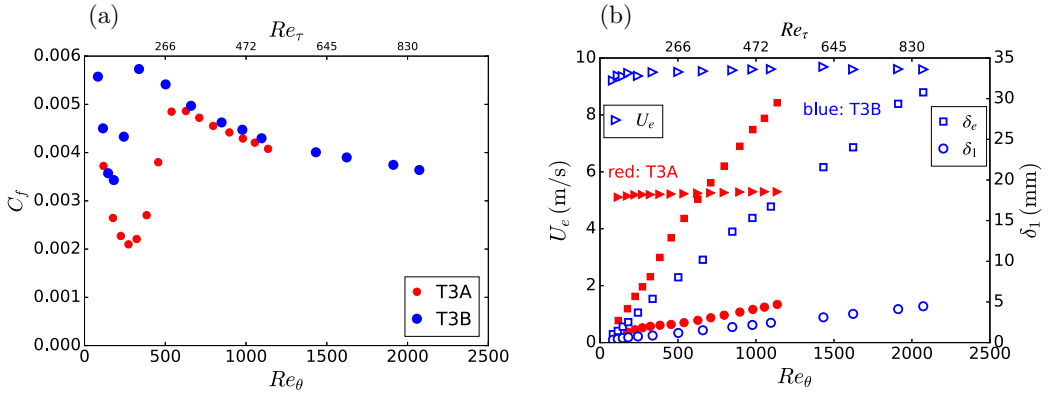

FIG. 2. (a) Friction coefficient vs Re_θ. (b) Free-stream velocity, boundary layer thickness, and mass displacement thickness. Experimental data are from Ref. [8], archived as case 20 in the European Research Community on Flow, Turbulence and Combustion (ERCOFTAC) database [9].

A. Experimental data

Accurately measuring the mean wall-normal velocity in experimental studies of boundary layer flows is challenging due to its small magnitude. Consequently, direct measurements of V_e are sparse and prone to uncertainties. If data of U_e and δ_1 are available across the x range, Eq. (6) can, however, be applied to compute V_e indirectly. In this paper, experimental data obtained from Ref. [8] were used to indirectly assess the validity of Eq. (9). These experiments were conducted at the Rolls-Royce Applied Science Laboratory and involved flat-plate transitional two-dimensional (2D) boundary layer flows. The boundary layers initially develop in a laminar state and then undergo a transition to turbulence at a specific distance downstream of the leading edge, depending on the turbulence level in the free stream and the leading-edge geometry. For our analysis, we employ two cases under zero pressure gradient, namely case T3A and case T3B.

Figure 2 presents key variables characterizing the two experiments. The friction factor $C_f = 2u_\tau^2/U_e^2$ is shown in Figs. 2(a) and 2(b) displays the free-stream velocity U_e, the boundary layer thickness δ_e, and the mass displacement thickness δ_1. Figure 2(a) highlights distinct transitions from laminar to turbulent flows for the two cases: Case T3A enters the turbulent regime at approximately $\mathrm{Re}_\theta \approx 540$ ($\mathrm{Re}_\tau \approx 250$), while case T3B enters at a lower Reynolds number of $\mathrm{Re}_\theta \approx 340$ ($\mathrm{Re}_\tau \approx 180$). Additionally, case T3A initiates the transition at approximately $\mathrm{Re}_\theta \approx 260$ ($\mathrm{Re}_\tau \approx 75$), exceeding case T3B's corresponding values of $\mathrm{Re}_\theta \approx 180$ ($\mathrm{Re}_\tau \approx 55$).

Figure 2(b) indicates that the free-stream velocity in case T3B is approximately twice that of case T3A. Consequently, the boundary layer thickness and mass displacement thickness in case T3B are thinner in comparison to case T3A. Due to the inherent uncertainties present in experimental studies, measurements of U_e or δ_e may not be completely smooth in the x direction, as shown in Fig. 2(b). This, in turn, leads to larger uncertainties when calculating x derivatives.

Figure 3 displays the four terms of integral equation (9) for the two experiments. It is important to note that V_e was not directly measured but was calculated using Eq. (6). The sum of the RHS of Eq. (9) closely approximates to $U_e V_e/u_\tau^2$, particularly in case T3B. There are, however, noticeable scatter and discrepancies. These could be attributed to (1) measurement uncertainties in u_τ, U_e, and δ_1 and (2) uncertainties in the calculation of x derivatives resulting from the distances between x-measurement stations being significantly greater than the local boundary layer thickness, especially at low Reynolds numbers where the boundary layer is thin. For instance, the distances between the initial x-measurement stations in case T3A or T3B may reach up to 20 times the local boundary layer thickness. Additionally, the measurement and calculation of Reynolds normal stress derivatives can introduce uncertainty and scatter.

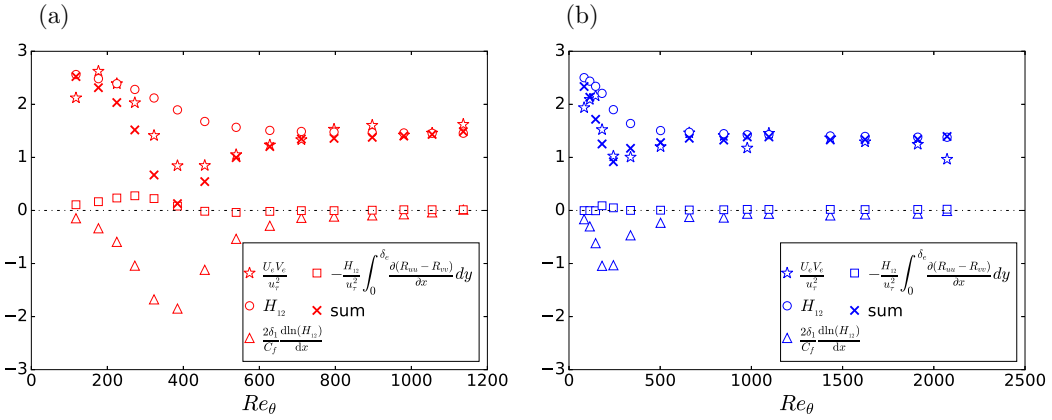

FIG. 3. Evaluating the validity of integral equation (9) using experimental data. (a) Case T3A. (b) Case T3B.

Even with these uncertainties, Fig. 3 provides clear evidence that the second term on the RHS of Eq. (9) holds significance during the transitional Reynolds number range, but diminishes to negligible magnitudes as the ZPG boundary layer flow progresses into fully turbulent states. On the other hand, the last term on the RHS of Eq. (9), originating from the Reynolds normal stresses, remains relatively small throughout.

B. Direct numerical simulation data

In theory, DNS data offer greater convenience for evaluating the accuracy of Eq. (9), as all the terms in the equation, including V_e, can be directly computed with high resolution and precision. However, exact calculation of x derivatives requires access to two-dimensional mean field data in a spatially developing boundary layer flow. Unfortunately, certain DNS databases of ZPG boundary layers only provide discrete Reynolds number data without specifying the corresponding x locations. While U_eV_e/u_τ^2 and H_{12} values can be obtained from such data (see Fig. 1), the necessary information to calculate $\mathrm{d}H_{12}/\mathrm{d}x$ or other x derivatives is generally lacking.

Wu and Moin [10] conducted a DNS study of a nominally zero-pressure-gradient boundary layer flow, covering the transition from the Blasius regime to turbulence. The transition to turbulence was initiated by periodic introduction of intermittent localized disturbances from the free stream at the inlet. The mean wall static pressure gradient, represented as C_{pw}, was maintained within the range 0–0.012 along the streamwise direction for $80 < \mathrm{Re}_\theta < 940$. However, near the exit, the convective outflow boundary condition led to a rapid increase in the magnitude of C_{pw} [10]. As a result, caution should be exercised when interpreting simulation results for $\mathrm{Re}_\theta > 1000$ in the DNS of Wu and Moin since they deviate from ZPG TBL behavior.

Figure 4(a) shows the variation of the friction coefficient, indicating transition initiation at $\mathrm{Re}_\theta \approx 240$ (or $\mathrm{Re}_\tau \approx 50$) and entry into the turbulent regime at $\mathrm{Re}_\theta \approx 780$ (or $\mathrm{Re}_\tau \approx 360$). Using the same DNS data set, Klewicki *et al.* [11] analyzed the leading-order balance structure of the mean momentum equation (3) and confirmed the onset of the four-layer structure identified by Wei *et al.* [12] at an estimated $\mathrm{Re}_\theta \approx 780$ (or $\mathrm{Re}_\tau \approx 360$).

Figure 4(b) presents the variations of U_eV_e/u_τ^2, H_{12}, and the correction term arising from $\partial U^-/\partial x^*$. The calculation of the correction term from $R_{uu} - R_{vv}$ was, however, not possible due to the unavailability of the relevant data. It is, nevertheless, assumed to be relatively small. The determination of V_e involves a higher level of uncertainty in comparison to other flow statistics, primarily due to the difficulty of precisely and consistently identifying the boundary layer edge [13]. In this paper, the boundary layer edge is determined as the location of $0.99U_e$.

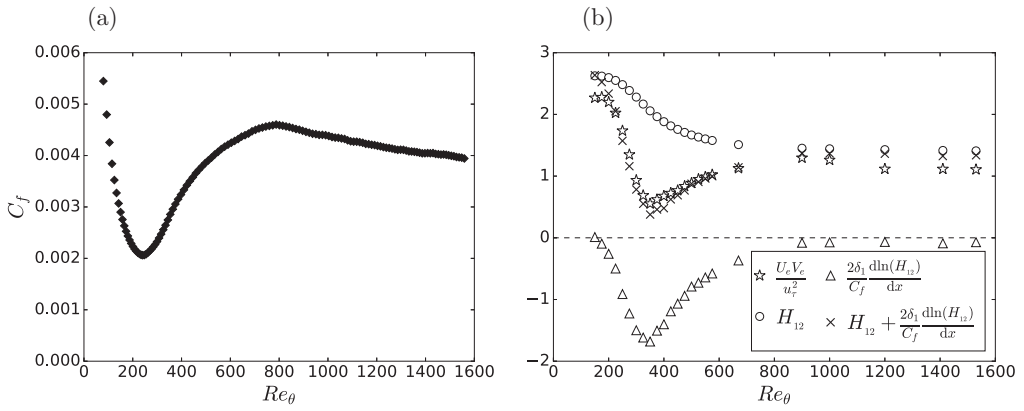

FIG. 4. DNS data of Wu and Moin [10]. (a) Friction coefficient vs Re_θ. (b) U_eV_e/u_τ^2, H_{12}, and the correction term from $\partial U^-/\partial x^*$.

Figure 4(b) shows that, overall, the DNS data from Wu and Moin [10] agree well with the analytical equation (9) for $\mathrm{Re}_\theta \lesssim 1000$. Across transitional Reynolds numbers, the significance of the second term on the right-hand side of Eq. (9) becomes apparent; yet this term tends to approach zero at $\mathrm{Re}_\theta \approx 1000$. Although the specific values of the third term are not available, the data in Fig. 4(b) suggest that its contribution is negligible.

In Fig. 4(b), a notable discrepancy can be seen between the calculated U_eV_e/u_τ^2 and H_{12}, with differences of up to 25% within the $1000 < \mathrm{Re}_\theta < 1600$ range. In contrast, the agreement between U_eV_e/u_τ^2 and H_{12} across the same range of Reynolds numbers is much better in the DNS study conducted by Schlatter and Örlü [3], as shown in Fig. 1. It is worth noting that Schlatter and Örlü's DNS deals with fully turbulent flow without simulating a transition from laminar to turbulence. Conversely, Wu and Moin's DNS [10] involved a complex transition from laminar to turbulent flow [10]. Interestingly, Elnahhas and Johnson [14] and Kianfar *et al.* [15], in their examination of the same DNS data set, observed a reversal in the direction of the mean wall-normal velocity during the transitional regime. Through the application of integral equations, they demonstrated that this velocity reversal significantly influences skin friction. How such a reversal could be physically realized is unclear, and likely highlights the challenges of simulating transitional flows.

IV. SUMMARY

This work presents an improved formulation of the integral relation proposed by Wei and Klewicki in 2016 [1] for ZPG boundary layer flows. The modification introduced in this analysis extends the applicability of the relation to arbitrary Reynolds numbers, spanning the laminar, transitional, and turbulent regimes. The examination of additional terms highlights their significance for transitional Reynolds numbers. In this regime, the development of time-averaged profiles is significantly affected by instability details, resulting in distinct values of C_f, δ_1, H_{12}, Reynolds normal stresses, and the associated correction terms. With increasing Reynolds number into the fully developed turbulent regime [12], the simple integral relation of Wei and Klewicki [1] is recovered with high precision according to comparisons with the experiments described by Roach and Brierlay [8] and the DNS of Schlatter and Örlü [3] and Simens *et al.* [4]. Furthermore, the improved integral relation can serve as a valuable tool for evaluating the accuracy of numerical simulations of the ZPG TBL, as it encapsulates the principles of mass and momentum conservation.

ACKNOWLEDGMENTS

We are grateful to Dr. Xiaohua Wu for generously sharing the DNS data and to the reviewers of the manuscript for their insightful comments. We also acknowledge the University of Manchester for housing the Classic Collection Database for ERCOFTAC. T.W. thanks Dr. Zhaorui Li for meticulous proofreading and valuable feedback.

The authors report no conflict of interest.

APPENDIX A: CORRECTION TERM FROM $\partial U^-/\partial x^*$

The first two terms on the RHS of Eq. (8) can be expressed as

$$\begin{aligned}-\int_0^{\delta_e}\frac{\partial U^2}{\partial x}\mathrm{d}y - U_eV_e &= -\left(\frac{\mathrm{d}}{\mathrm{d}x}\int_0^{\delta_e}U^2\mathrm{d}y - U_e^2\frac{\mathrm{d}\delta_e}{\mathrm{d}x}\right) - U_e^2\frac{\mathrm{d}\delta_1}{\mathrm{d}x}\\ &= -\left(\frac{\mathrm{d}}{\mathrm{d}x}\left[U_e^2(\delta_e-\delta_1-\delta_2)\right] - U_e^2\frac{\mathrm{d}\delta_e}{\mathrm{d}x}\right) - U_e^2\frac{\mathrm{d}\delta_1}{\mathrm{d}x}\\ &= U_e^2\frac{\mathrm{d}\delta_2}{\mathrm{d}x}. \end{aligned} \tag{A1}$$

Note that by definition, $\int_0^{\delta_e}U^2\mathrm{d}y = U_e^2(\delta_e-\delta_1-\delta_2)$. Also, $U_e^2\mathrm{d}\delta_2/\mathrm{d}x$ represents the classic Kármán integral for the ZPG TBL (see Ref. [2]), which can be rearranged as follows:

$$U_e^2\frac{\mathrm{d}\delta_2}{\mathrm{d}x} = U_e^2\frac{\mathrm{d}(\delta_1/H_{12})}{\mathrm{d}x} = U_e^2\frac{H_{12}\frac{\mathrm{d}\delta_1}{\mathrm{d}x} - \delta_1\frac{\mathrm{d}H_{12}}{\mathrm{d}x}}{H_{12}^2} = \frac{U_eV_e}{H_{12}} - \frac{U_e^2\delta_1}{H_{12}^2}\frac{\mathrm{d}H_{12}}{\mathrm{d}x}. \tag{A2}$$

Note that Eq. (6) is used to write $U_e^2\mathrm{d}\delta_1/\mathrm{d}x$ as U_eV_e. Substituting Eq. (A2) back into the momentum integral equation (8) and multiplying both sides by H_{12}/u_τ^2 results in

$$\frac{U_eV_e}{u_\tau^2} = H_{12} + \frac{2\delta_1}{C_f}\frac{\mathrm{d}\ln(H_{12})}{\mathrm{d}x} - \frac{H_{12}}{u_\tau^2}\int_0^{\delta_e}\frac{\partial(R_{uu}-R_{vv})}{\partial x}\mathrm{d}y. \tag{A3}$$

In ZPG laminar boundary layer flow, $H_{12}\approx 2.59$ remains constant, resulting in the second term on the RHS of Eq. (9) becoming identically zero. In the ZPG TBL, as the Reynolds number increases, H_{12} decreases while δ_1 increases. These variations are generally gradual, except within the transitional Reynolds number range. Figure 5 shows the variations of $2\delta_1\,\mathrm{d}\ln(H_{12})/\mathrm{d}x$ and C_f with Reynolds numbers. At large Reynolds numbers, say, $\mathrm{Re}_\theta \gtrsim 1000$, $2\delta_1\,\mathrm{d}\ln(H_{12})/\mathrm{d}x$ approaches zero. Consequently, the second term on the RHS of Eq. (9) also becomes negligible, as shown in Fig. 3. However, over the transitional regime, this term remains significant and cannot be neglected.

To elucidate the source of the corrective term $(2\delta_1/C_f)\mathrm{d}\ln(H_{12})/\mathrm{d}x$, we can reformulate Eq. (A1) as

$$\begin{aligned}-\int_0^{\delta_e}\frac{\partial U^2}{\partial x}\mathrm{d}y - U_eV_e &= -\int_0^{\delta_2}2U\frac{\partial U}{\partial x}\mathrm{d}y - U_eV_e\\ &= -\int_0^1 2(U_e-U_eU^-)\left(\frac{U_e}{\delta_e}\frac{\mathrm{d}\delta_e}{\mathrm{d}x}y^- - \frac{\partial U^-}{\partial y^-} - \frac{U_e}{L}\frac{\partial U^-}{\partial x^*}\right)\delta_e\mathrm{d}y^- - U_eV_e \end{aligned} \tag{A4}$$

and represent V_e in the following form (refer to Ref. [6] for more details):

$$V_e = U_e\frac{\mathrm{d}\delta_e}{\mathrm{d}x}\frac{\delta_1}{\delta_e} + U_e\frac{\delta_e}{L}\int_0^1\frac{\partial U^-}{\partial x^*}\mathrm{d}y^-. \tag{A5}$$

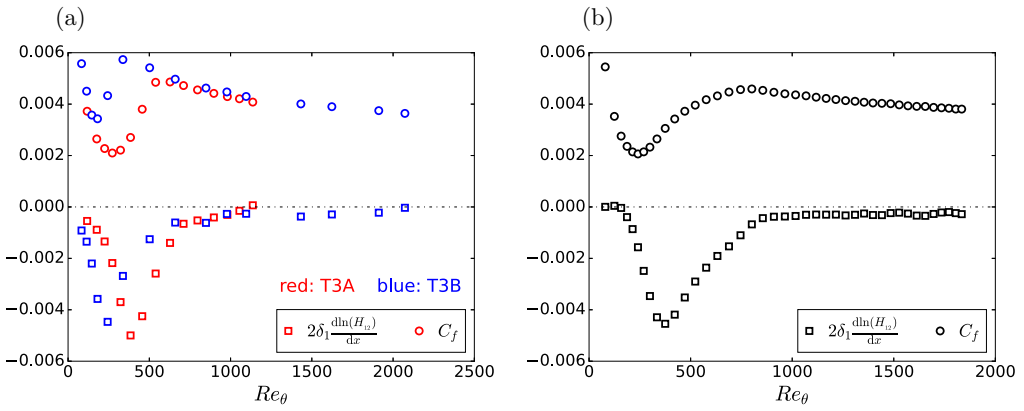

FIG. 5. Variation of $2\delta_1\,\mathrm{d}\ln(H_{12})/\mathrm{d}x$ and C_f. (a) Experimental data from experiments of Ref. [8]. (b) DNS data from Ref. [10].

Following straightforward mathematical steps, the global integral of the advective terms can be formulated as follows:

$$-\int_0^{\delta_e}\frac{\partial U^2}{\partial x}\mathrm{d}y - U_eV_e = U_e^2\frac{\mathrm{d}\delta_e}{\mathrm{d}x}\frac{\delta_2}{\delta_e} + U_e^2\frac{\delta_e}{L}\left(\int_0^1\frac{\partial U^-}{\partial x^*}\mathrm{d}y^- - \int_0^1\frac{\partial (U^-)^2}{\partial x^*}\mathrm{d}y^-\right). \tag{A6}$$

We rearrange the first term in Eq. (A6) as

$$U_e^2\frac{\mathrm{d}\delta_e}{\mathrm{d}x}\frac{\delta_2}{\delta_e} = \left(U_e^2\frac{\mathrm{d}\delta_e}{\mathrm{d}x}\frac{\delta_1}{\delta_e}\right)\frac{\delta_2}{\delta_1} = \left(U_eV_e - U_e^2\frac{\delta_e}{L}\int_0^1\frac{\partial U^-}{\partial x^*}\mathrm{d}y^-\right)\frac{1}{H_{12}}. \tag{A7}$$

Therefore it can be demonstrated that the origin of the correction term $(\frac{2\delta_1}{C_f})\,\mathrm{d}\ln(H_{12})/\mathrm{d}x$ arises from the $\partial/\partial x^*$ components.

APPENDIX B: CORRECTION FROM REYNOLDS NORMAL STRESSES

The Leibniz integral rule allows one to show that the last term in Eq. (A3) can be written as

$$\begin{aligned}
&-\frac{H_{12}}{u_\tau^2}\int_0^{\delta_e}\frac{\partial(R_{uu}-R_{vv})}{\partial x}\mathrm{d}y \\
&= -\frac{H_{12}}{u_\tau^2}\left(\frac{\mathrm{d}}{\mathrm{d}x}\int_0^{\delta_e}(R_{uu}-R_{vv})\mathrm{d}y - (R_{uu}(\delta_e)-R_{vv}(\delta_e))\frac{\mathrm{d}\delta_e}{\mathrm{d}x}\right) \\
&= -\frac{H_{12}}{u_\tau^2}\frac{\mathrm{d}}{\mathrm{d}x}\int_0^{\delta_e}(R_{uu}-R_{vv})\mathrm{d}y \;+\; H_{12}(R^+_{uu}(\delta_e)-R^+_{vv}(\delta_e))\frac{\mathrm{d}\delta_e}{\mathrm{d}x} \\
&= -\frac{H_{12}}{u_\tau^2}\frac{\mathrm{d}}{\mathrm{d}x}\left(u_\tau^2\delta_e\int_0^1(R^+_{uu}-R^+_{vv})\mathrm{d}y^-\right) \;+\; H_{12}(R^+_{uu}(\delta_e)-R^+_{vv}(\delta_e))\frac{\mathrm{d}\delta_e}{\mathrm{d}x}.
\end{aligned} \tag{B1}$$

Here, R^+_{uu} and R^+_{vv} represent the inner-scaled Reynolds normal stresses, defined as R_{uu}/u_τ^2 and R_{vv}/u_τ^2, respectively. Typically, the Reynolds normal stresses at the boundary layer edge are small, resulting in a small second term in the last line of Eq. (B1). Figure 6 illustrates the relationship between the integrals of $\langle uu\rangle^+$ and $\langle vv\rangle^+$ as a function of Reynolds numbers. In the transitional regime, the integrals show significant variations with changes in Reynolds number or x location.

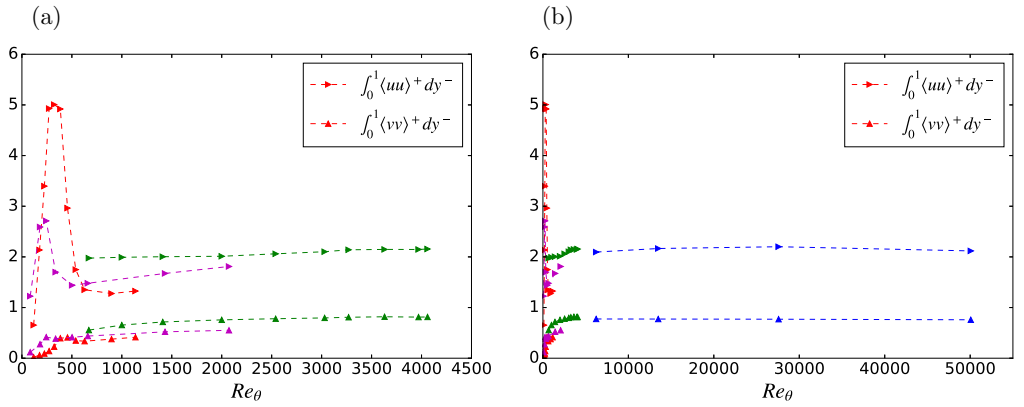

FIG. 6. Integrals of $\langle uu \rangle^+$ and $\langle vv \rangle^+$ vs Reynolds numbers. (a) Low and moderate Reynolds numbers. (b) Over a wider range of Reynolds numbers. Data symbols: red, T3A in Ref. [8]; magenta, T3B in Ref. [8]; green, DNS from Ref. [16]; blue, experimental data from Ref. [17].

However, as the Reynolds numbers increase to sufficiently high values, the variations of the integrals diminish to negligible values.

[1] T. Wei and J. Klewicki, Scaling properties of the mean wall-normal velocity in zero-pressure-gradient boundary layers, Phys. Rev. Fluids **1**, 082401(R) (2016).

[2] H. Schlichting, *Boundary-Layer Theory* (McGraw-Hill, New York, 1979).

[3] P. Schlatter and R. Örlü, Assessment of direct numerical simulation data of turbulent boundary layers, J. Fluid Mech. **659**, 116 (2010).

[4] M. P. Simens, J. Jiménez, S. Hoyas, and Y. Mizuno, A high-resolution code for turbulent boundary layers, J. Comput. Phys. **228**, 4218 (2009).

[5] A. A. Townsend, *The Structure of Turbulent Shear Flow* (Cambridge University Press, Cambridge, 1956).

[6] T. Wei, Z. Li, and Y. Wang, New formulations for the mean wall-normal velocity and Reynolds shear stress in turbulent boundary layer under zero pressure gradient, J. Fluid Mech. **969**, A3 (2023).

[7] H. Tennekes and J. L. Lumley, *A First Course in Turbulence* (MIT Press, Cambridge, MA, 1972).

[8] P. E. Roach and D. H. Brierlay, The influence of a turbulent free-stream on zero pressure gradient transitional boundary layer development including the conditions test cases T3A and T3B, in *Numerical Simulation of Unsteady Flows and Transition to Turbulence*, edited by O. Pironneau, W. Rodi, I. L. Ryhming, A. M. Savill, and T. V. Truong (Cambridge University Press, Cambridge, 1990), pp. 319–347.

[9] http://cfd.mace.manchester.ac.uk/ercoftac/doku.php?id=cases:case020.

[10] X. Wu and P. Moin, Direct numerical simulation of turbulence in a nominally zero-pressure-gradient flat-plate boundary layer, J. Fluid Mech. **630**, 5 (2009).

[11] J. Klewicki, R. Ebner, and X. Wu, Mean dynamics of transitional boundary-layer flow, J. Fluid Mech. **682**, 617 (2011).

[12] T. Wei, P. Fife, J. Klewicki, and P. McMurtry, Properties of the mean momentum balance in turbulent boundary layer, pipe and channel flows, J. Fluid Mech. **522**, 303 (2005).

[13] T. Wei, Z. Li, T. Knopp, and R. Vinuesa, The mean wall-normal velocity in turbulent-boundary-layer flows under pressure gradient, J. Fluid Mech. **975**, A27 (2023).

[14] A. Elnahhas and P. L. Johnson, On the enhancement of boundary layer skin friction by turbulence: An angular momentum approach, J. Fluid Mech. **940**, A36 (2022).

[15] A. Kianfar, A. Elnahhas, and P. L. Johnson, Quantifying how turbulence enhances boundary layer skin friction and surface heat transfer, AIAA J. **61**, 3900 (2023).
[16] M. K. Lee and R. D. Moser, Direct numerical simulation of turbulent channel flow up to $Re_\tau = 5200$, J. Fluid Mech. **774**, 395 (2015).
[17] R. Baidya, J. Philip, N. Hutchins, J. P. Monty, and I. Marusic, Spanwise velocity statistics in high-Reynolds-number turbulent boundary layers, J. Fluid Mech. **913**, A35 (2021).